BNL-221076-2021-JAAM

Size and Stoichiometry Effects on the Reactivity of MoCy Nanoparticles Towards Ethylene

C. Jimenez-Orozco, J. A. Rodriguez

To be published in "Journal of Physical Chemistry C"

February 2021

Chemistry Department

Brookhaven National Laboratory

U.S. Department of Energy

USDOE Office of Science (SC), Basic Energy Sciences (BES) (SC-22)

DISCLAIMER

Size and Stoichiometry Effects on the Reactivity of MoC_y Nanoparticles Towards Ethylene

Carlos Jimenez-Orozco,*[a] Marc Figueras,[b] Elizabeth Florez,[a] Francesc Viñes,[b] José A. Rodriguez,[c] Francesc Illas*[b]

[a] *Universidad de Medellín, Facultad de Ciencias Básicas, Grupo de Materiales con Impacto (Mat&mpac), Carrera 87 No 30-65, Medellín, Colombia*

[b] *Universitat de Barcelona, Departament de Ciència de Materials i Química Física & Institut de Química Teòrica i Computacional (IQTCUB), c/ Martí i Franquès 1-11, 08028 Barcelona, Spain.*

[c] *Brookhaven National Laboratory, Chemistry Department, Upton, New York 11973, United States of America*

Abstract

Molybdenum carbides are promising catalysts alternative to Pt-group metals for the hydrogenation of unsaturated hydrocarbons. Nanostructuring has been shown to be an efficient way to boost the catalytic activity of these materials with MoC_y nanoparticles (NPs) exhibiting a good performance when encapsulated inside zeolites or dispersed on inert supports such as carbon or gold. Hereby, we focus on a systematic DFT study of the interaction of MoC_y NPs with ethylene (C_2H_4), as a general and simple approach for examining binding and activation of C═C bonds. Models for 14 NPs, with a Mo/C ratio in the 0.67 to 2.00 range, have been built following a cascade procedure. Several chemical descriptors, including the adsorption energy, structural NPs distortion, C═C deformation, and C_2H_4 attachment energy have been analyzed along with a meticulous geometric and electronic characterization of bare NPs and C_2H_4 binding. The present results show that 1:1 stoichiometric Mo_6C_6, $Mo_{12}C_{12}$, and $Mo_{24}C_{24}$, and the non-stochiometric Mo_4C_6, Mo_8C_{12} (MetCar), and $Mo_{14}C_{13}$ (Nanocube) are excellent systems for the binding and activation of ethylene, exhibiting a much bigger reactivity than a bulk δ-MoC(001) surface with a similar Mo:C ratio. In addition, C_2H_4 binding on the NPs with a Mo/C < 1.08 is advantageous since, apart from a rather large adsorption energy, implies low energy values for NPs deformation (from 0.00 to 0.31 eV), C═C distortion (from 0.30 to 0.52 eV), and C_2H_4 attachment (from -2.12 to -2.58 eV). These theoretical results point to the ideal MoC_y size and composition for C_2H_4 binding, providing a background for further experimental studies aimed at the preparation of MoC_y NPs as hydrogenation catalysts.

* Corresponding authors: cjimenez@udem.edu.co, francesc.illas@ub.edu

1. Introduction

The use of catalysts is key for producing clean fuels and several commodities, particularly by means of hydrogenation reactions of C═C double bonds in olefins, where Pt, Pd, Ru, Rd, Os, and Ir —sometimes referred to as Pt-group elements— are so far the most used catalyst due to their good performance.[1] In practice, these metals are supported on oxides, zeolites, and activated carbon, and exhibit a high catalytic activity.[2-11]. However, the scarcity of these metals in the Earth crust, together their sensitivity to sulfur poisoning in the petrochemical industry, has motivated the search for alternative catalysts.[2]

Several studies have shown that transition metal carbides have excellent catalytic properties and appear as a good alternative to replace Pt-group based catalysts, especially on several hydrogenation reactions. Among them, molybdenum carbides are highlighted as promising materials, due to their remarkable interaction with hydrocarbons and with several successful applications in hydrogenation reactions. [12-16] Not surprisingly, several studies have been reported on the interaction of C_2H_4 with molybdenum carbides surfaces, precisely to explore the capability of these materials as potential alternative catalysts to Pt-group metals.[17-20] The binding and hydrogenation of the ethylidyne species on δ-MoC(001) has also been considered,[20] since these species have been found to be responsible of poisoning in Pt-based catalysts. Interestingly, there is evidence that this material could avoid surface poisoning, in contrast to Pt and Pd extended surfaces.[20]

The good performance of molybdenum carbides in catalysis has triggered new research aimed at investigating their possible improvement by nanostructuring. Recently, Figueras *et al.*[21] presented experimental and theoretical evidence that MoC_y nanoparticles supported on Au(111) can dissociate methane at room temperature. Additionally, this inverse catalyst system appears to be a good candidate for hydrogenation reactions as H_2 can easily dissociate and be stored on the supported nanoparticles[22] in a rather broad temperature range. Both, the activation of methane and the activity towards hydrogen suggest that these nanoparticles (NPs) could be useful for hydrogenation of olefins. In addition, MoC_y NPs can be easily synthesized[23] thus overcoming the problems encountered when aiming at preparing MoC or Mo_2C single crystal surfaces. Furthermore, it is known that MoC_y NPs encapsulated inside zeolites or dispersed on supports such as carbon or oxides exhibit good catalytic properties.[24-27]

At the present time, very little is known about the intrinsic reactivity of MoC_y NPs towards olefins or unsaturated hydrocarbons in general. The fact that the MoC_y NPs are frequently dispersed on zeolites, oxides, metals and carbon-based supports raises the question about the possible influence of the substrate on their intrinsic chemical properties. To answer this question, we have carried out a computational study, based on density functional theory (DFT), aimed at examining the bonding and activation of ethylene on a series of MoC_y NPs with different shapes and Mo:C atomic ratios; ethylene can be taken as a model for larger olefins. Our results show that the MoC_y NPs display a behavior which cannot be extrapolated from those seen for bulk δ-MoC(001) and β-Mo_2C(001) surfaces, with a substantial boost in chemical activity.

2. Nanoparticles Models and Computational Details

The interaction of ethylene (C_2H_4) with gas-phase MoC_y NPs has been studied using a series of models of increasing size, considering also different stoichiometries, as shown in Figure 1. The NPs models contain up to 64 atoms where the Mo/C ratio varies from 0.67 to 2.00. Note that this comprises usual MoC and Mo_2C stoichiometries, as well as C-rich NPs like the well-known Mo_8C_{12} MetCar. The initial stoichiometric structures of MoC_y nanoparticles have been obtained from different sources. For instance, the Mo_6C_6 and $Mo_{12}C_{12}$ NPs have been gained by mimicking most stable gas-phase TiC NPs as previously reported.[28] These were acquired through data mining searches, global optimization using Interatomic Potentials (IP), and subsequent geometry optimization by DFT calculations. There, the authors reported a total of 21 low energy structures for each Ti_6C_6 and $Ti_{12}C_{12}$ stoichiometry. Here, these TiC NP structures have been used as templates, substituting Ti by Mo and fully re-optimizing the atomic structure using the methodology described below. Remarkably, the shape of most stable MoC_y isomers of both sizes coincides with that of their TiC counterparts. This is not surprising as both TiC and the δ-MoC polymorph exhibit the same rock-salt structure. This bottom-up approach revealed a quite fast convergence towards to cubic, δ-MoC bulk-like shapes. Thus, a complementary top-down approach has been also considered creating cubic-like arrangements for $Mo_{24}C_{24}$ and $Mo_{32}C_{32}$ NPs, following a Wulff construction shape[29] and relying on the computed δ-MoC surface energies.[30,31]

Moreover, non-stoichiometric NPs have been considered and built from different sources as well. First, the Mo_8C_{12} magic cluster, usually known as MetCar,[32] and the $Mo_{14}C_{13}$ nanocube,[33] have been selected from the literature. Then, other small MoC_y clusters have been considered through a cascade procedure, where for the two most stable isomers of Mo_6C_6 and $Mo_{12}C_{12}$ all inequivalent atoms have been sequentially removed generating different $Mo_{x-1}C_x$ or Mo_xC_{x-1} structures. After optimizing the resulting structures, the cascade procedure is repeated to reach suitable structures for other Mo/C ratios. This methodology approximately scales as $2 \cdot N^Z$ per removal, where N is the average number of inequivalent atoms per removal, Z states for the number of atoms that have been already removed, and the coefficient 2 is necessary as there are two different kinds of species. For instance, seven inequivalent C atoms exist for the most stable $Mo_{12}C_{12}$ isomer. Thus, removing one atom leads to 7 structures and a second removal leads to 49 new structures that need to be considered for subsequent geometry optimization. In any case, the actual number of isomers to explore on each batch depends on the new number of inequivalent atoms, yet the adoption of particularly symmetric shapes may reduce this number. Regardless of the previous, the $2 \cdot N^Z$ expression should be taken as an upper bound. Clearly, a full cascade procedure becomes computational prohibitive for *Z* larger than two, especially for larger NPs such as $Mo_{12}C_{12}$. Thus, further *Z* steps have been explored only departing from the *Z*-1 most stable isomer. This strategy is not entirely arbitrary, as systematically for the first round the most stable isomers are obtained from previous most stable ones.

The total energy of the studied MoC_y models described in the previous subsection has been obtained through periodic Density Functional Theory (DFT) calculations using large enough supercells so that the interaction between the periodically repeated nanoparticles become negligible. Thus, the MoC_y nanoparticles have been placed inside a large cubic box, ensuring a minimum vacuum region of 10 Å in all directions and, obviously, considering the **Γ** point only. The calculations were carried out using the Vienna *Ab Initio* Simulation Package (VASP) code,[34] employing the Perdew-Burke-Ernzerhof (PBE) exchange-correlation functional,[35] as found to be especially well-suited in the description of Mo-based carbides.[36] In addition, the contribution of dispersion terms was accounted adding the Grimme D3 correction, *i.e.* PBE-D3,[37] especially adequate for the interaction of molecules with such molybdenum carbide systems.[19,36,38,39] The Kohn-Sham equations were solved by expanding the valence electron density in a plane-wave basis set with 415 eV cutoff whereas the effect of the inner electrons in the valence electron density has been taken into account by the Projected Augmented Wave (PAW) method[40] as implemented by Kresse and Joubert.[41] The convergence criteria were changes in total energies lower than 10^{-5} eV and variations in interatomic forces lower than 0.01 $eV \cdot Å^{-1}$. With this setup, total energies converge below the chemical accuracy of 1 $kcal \cdot mol^{-1}$ —i.e. ~0.04 eV.

Regarding the approach used to choose of the structures of the MoCy NPs described above, one must acknowledge recent proposals in the literature aimed at exploring the landscape for several isomers.[42-44] These rely on geometry optimization and consideration of low-lying isomers, being able to scrutinize the role of possible higher energy isomers in a given reaction at a given temperature. These approaches can provide detailed information about the contribution of each isomer to the overall reactivity. Nevertheless, the importance of high energy isomers becomes relevant for subnanometer NPs only and, in general, becomes less and less important for larger NPs where the energy difference between structural isomers gradually increase with the NP size, see Table S1 of the SI. In addition, exploring the importance of different isomers for a set of nanoparticles becomes computationally too demanding and is, hence, beyond of the scope of the present work. Yet, the present approach, focusing on relatively low energy isomers, hopefully close to the global minima, allows one to extract meaningful information about the chemistry of these catalytically active MoC_y

nanoparticles. Consequently, for each stoichiometry, the most stable cluster was selected to analyze the interaction with ethylene.

Once the optimum structure of the MoC_y NPs has been obtained, the interaction of each of them with the C_2H_4 molecule has been studied using the same computational setup. All conceivable binding sites and connectivities have been explicitly considered. The notation for the adsorption modes is as earlier reported.[17,18,45] Briefly, π-M relates to ethylene binding atop of a metal site; di-σ-MM, di-σ-CM, and di-σ-CC correspond to the binding bridging metal-metal, carbon-metal, and carbon-carbon bond, respectively and; finally, σ-M, μ-M stands for a situation in which one has one C atom of C_2H_4 atop of a metal atom (σ-M) and one C_2H_4 C atom located perpendicularly atop of a M-M bridge (μ-M). For every NP, several initial adsorption geometries where evaluated to cover all binding possibilities, so that a complete scanning of the potential energy surface for C_2H_4 binding in every NP can be assured. In total, the number of studied initial adsorption geometries was of *circa* 500. The final structures —bare nanoparticles and nanoparticles with adsorbed ethylene— were characterized as energy minima in the potential energy surface through pertinent vibrational analysis. The vibrational frequencies were gained within the harmonic approximation, accounting only the adsorbate vibrational frequencies, obtained through the building up and diagonalization of the Hessian matrix, constructed by finite differences of analytical gradients with atomic displacements of 0.03 Å.

The ethylene adsorption energy, E_{ads}, was calculated as

$$E_{ads} = E_{C_2H_4/MoC_y} - E_{MoC_y} - E_{C_2H_4} \quad (1),$$

where $E_{C_2H_4/MoC_y}$ stands for the energy of the system with the C_2H_4 adsorbed on the MoC_y NP, the term E_{MoC_y} refers to the MoC_y optimized energy, while $E_{C_2H_4}$ represents the isolated ethylene molecular energy. The first and third terms in Eq. (1) include the ethylene related vibrational Zero-Point Energy (*ZPE*) contribution.

To investigate the bonding between ethylene and the MoC_y nanoparticles, a Charge Density Difference (*CDD*) analysis, Δρ, has been carried out, along with the Electron Localization Function (*ELF*). In the CDD Δρ is defined as

$$\Delta\rho = \rho_{C_2H_4/MoC_y} - \rho_{MoC_y} - \rho_{C_2H_4} \quad (2),$$

where $\rho_{C_2H_4/MoC_y}$ refers to the electron density of the ethylene adsorbed on the MoC_y NP, and ρ_{MoC_y} and $\rho_{C_2H_4}$ correspond the electron density of the nanoparticle and ethylene at the geometry they have in the adsorbed minimum. In addition, net charges on the adsorbed molecule are also obtained through the Atoms-in-Molecules topological analysis of Bader.[46]

3. Results and discussion

3.1. Geometry and characterization of bare MoC_y nanoparticles

In Figure 1, the arrangement of carbon and molybdenum atoms within the MoC_y NPs is found to be different for each Mo/C ratio, and even for the same Mo/C ratio the relaxed geometries can be completely different. Thus, being in the non-scalable regime of NPs sizes,[29,47] their performance towards the binding of adsorbates is expected to be significantly different between the explored NPs. The geometries for the most stable structures of each of the 14 MoC_y NPs are the ones displayed in Figure 1. In order to separate stoichiometry from size effects, the MoC_y NPs analysis is split into stoichiometric and non-stoichiometric cases. The employed descriptors to unveil the properties of bare NPs are formation energies, computed taking the energy per atom in bulk Mo and graphite as atomic references, respectively —see Figure S1 and Table S2 of the SI— and the band gap, see Tables S2 and S3 of SI, which open the door towards the geometry and electronic properties characterization, respectively.

As far as stability is concerned, we first focus on the formation energy, E_{form}, as this quantity provides an estimate of the thermodynamic stability of a given NP, either stoichiometric or not. However, to have a meaningful comparison it is convenient to somehow normalize this quantity. For the stoichiometric NPs this can be done simply by considering E_{form} per MoC unit —*i.e.* E_{form}/N—. Here, a clear size effect is found where E_{form} linearly decreases as the size grows, see Table S2 and Figure S1 in SI. Interestingly, the band gap, E_{gap}, estimated in an approximate way from the Kohn-Sham orbital energies, exhibits a much less marked dependence with respect to the NP size and irrespective of whether these are stoichiometric or not; see Tables S2 and S3 in SI. For all NPs E_{gap} is close to 0.15 eV although with some oscillations of the energy levels that eventually lead to the valence and conduction band limits. In any case, from the calculated E_{gap} for these NPs, it is clear that they are still a bit far from metallic character predicted for the extended δ-MoC (001) surface.[31] Test studies were carried out for Mo_6C_6 and the MetCar, which are representative of stoichiometric and non-stoichiometric NPs, to calculate E_{gap} using the range-separated hybrid HSE06 functional. In both cases, the changes with respect to the PBE value are of 0.01 eV only.

Assuming that the frontier orbitals dominate the chemistry of these NPs, one would deduce that the binding of adsorbates on stoichiometric NPs in the range from Mo_6C_6, to $Mo_{32}C_{32}$ will be quite similar. However, the adsorbate binding strength does also depend on other factors, including *i)* the adsorbate nature, *ii)* the electronic arrangement with respect the NP model, *iii)* the anchoring site, and even *iv)* the adsorbate molecular conformation.

3.2. C_2H_4 adsorbed on MoC_y nanoparticles

Once all 14 stoichiometric MoC_y NPs were described, a thorough exploration sampling *ca.* 500 different initial C_2H_4 adsorption geometries was performed, covering all conceivable binding possibilities, revealing 221 final topologically different structures. The subsequent analysis, however, focuses on most stable adsorption conformation for each NP, as summarized in Table 1, and shown in Figure 2. Note that, for each case, the second most stable adsorption conformations are located more than 0.1 eV higher in energy —see Table S5 in SI—,with the sole exception of the MetCar, with rotated conformers around the NP tetrahedron vertex axis. Indeed, in most of the explored NPs, the second isomer is less stable by at least 0.2 eV, a behavior observed in 62% of the NPs listed in Table S5. However, one must advert that in 38% of NPs the adsorption conformations for both first and second most stable adsorption modes should be thermally accessible at the high temperatures typical in catalytic experiments; particularly, for C_2H_4 binding on Mo_5C_6, $Mo_{12}C_8$, $Mo_{12}C_{10}$, Mo_8C_{12}, and $Mo_{32}C_{32}$. Therefore, future studies should carefully address the existence of low lying isomers and possibly include them whenever considering the reactivity of these systems. For NPs with a 1:1 atomic ratio, the E_{ads} values are sensibly stronger than on the δ-MoC(001) surface, but within the range of values found for C- and Mo-terminated surfaces of β-Mo_2C(001) surfaces, as seen in Figure 3. The results in this figure indicate that the binding capabilities of the MoC_y NPs cannot be extrapolated from the behavior of the bulk δ-MoC(001) and β-Mo_2C(001) surfaces.

For comparison purposes, the C_2H_4 adsorption on extended δ-MoC(001) and C- and Mo-terminated β-Mo_2C(001) surfaces, denoted as β-Mo_2C(001)-C and β-Mo_2C(001)-Mo, are included in Table 1.[17-19] The adsorption energies, E_{ads}, on the NPs are in the -1.54 to -2.88 eV range, comparable to the strong binding on polar β-Mo_2C(001)-Mo surfaces, ranging -1.63 to -2.50 eV. On the other hand, the E_{ads} on polar β-Mo_2C(001)-C —with E_{ads} from -1.29 to -1.49 eV— and on the δ-MoC (001) surfaces —with E_{ads} up to -1.03 eV— are clearly weaker than on the studied NPs. Thus, the C_2H_4 E_{ads} binding strength decays as β-Mo_2C(001)-Mo ≈ NPs > β-Mo_2C(001)-C > δ-MoC(001). Notice that for the latter, the most stable reconstructed surface has been used as reference.[21] Interestingly, the reported values for C_2H_4 adsorption energy on a Pt(111) surface, -1.78 eV,[45] and on Pt_x (x = 7 – 10) clusters, ranging from -1.4 to -1.7 eV,[48,49] are within the range found in this work for the MoC_y NPs. Notice that the adsorption energy on platinum clusters and the Pt(111) surface is very similar which is in agreement with their similar catalytic performance towards ethylene hydrogenation.[50] In other words, nanostructuring Pt could not be advantageous for this particular hydrogenation process. However, a different behavior exists when comparing ethylene adsorption on MoC_y NPs and on TMC surfaces, where the current work is the basis to further explore this possibility.

Analyzing the adsorptive landscape in Table 1, the most common binding mode is π-M, closely followed by σ-M, μ-M, unfolding the main role played by Mo metal centers. The analogous geometry sites for binding on surfaces[17,18] is shown in Figure 4. Metal sites involved in bridge di-σ-CM are dominant on $Mo_{10}C_{12}$ and $Mo_{32}C_{32}$, while bridge di-σ-CC is only found for Mo_5C_6 case. Indeed, C-interaction is only found for Mo/C ratio of 0.8, with the sole exception of the $Mo_{32}C_{32}$ nanoparticle. The C_2H_4 preference towards Mo seems to be ruled by its lower electronegativity compared to C.[24]

The strong C_2H_4 adsorption on the NPs implies an elongation of the C═C double bond, *d*(CC), estimated to be 1.33 Å in gas phase. The *d*(CC) thus elongates from 0.09 to 0.25 Å for the studied NPs, see values in Table 1 and Table S4, and the largest elongations are found for MoC_y NPs involving C binding modes, such as in Mo_5C_6, $Mo_{10}C_{12}$, and $Mo_{32}C_{32}$, with elongations of 0.22 to 0.25 Å. The C_2H_4 binding involving two Mo sites *via* σ-M, μ-M mode display still moderate elongations of 0.15–0.18 Å, while π-M mode has a smaller, yet still noticeable lengthening of 0.09–0.10 Å. In this sense, the C_2H_4 carbon-carbon bond length distortion decreases with the binding mode as di-σ-CC, di-σ-CM > σ-M, μ-M > π-M. Notice in Table 1 that *d*(CC) bond length elongations are linked to the adsorption mode, rather than to its strength.

3.3. Analysis of C_2H_4 interaction with stoichiometric MoC_y NPs

In this section we analyze the chemical nature of C_2H_4 adsorption on stoichiometric MoC_y NPs. At first sight, there is no clear trend for adsorption energy evolution with respect NP size, having ups and downs, as seen in Figure 5. This behavior could be explained because the interaction is a balance of energy contributions, including: *i)* the C_2H_4 distortion energy when adsorbed, E_{dis}, as seen in the elongated *d*(CC) values of Table 1; *ii)* the NP deformation energy, E_{def}, so as to better accommodate the C_2H_4 moiety and the concomitant changes in the NP; and *iii)* the resulting attachment energy, E_{att}, as the binding energy of the distorted C_2H_4 on the deformed MoC_y NP, following a lock-and-key anchoring. The three different contributions are listed in Table S6 of the SI, revealing that the oscillations in the E_{ads} are also observed in the E_{att}, which is reminiscent of the fact that the studied NPs are in the non-scalable regime.[29] In any case, a slight trend is observed in Figure 5, as E_{ads} decreases as the NP size increases. Here the size is measured by $N^{-1/3}$, N being the number of MoC units —see also Table S7 in SI—. Figure 5 also reports the effect of non-stoichiometry for Mo_6C_6 and $Mo_{12}C_{12}$, where it clearly can be stated that the presence of Mo or C vacancies strengthen the adsorption.

Apart from the E_{ads} evolution, the size and attachment energy are useful descriptors to unveil the behavior of stoichiometric NPs as shown in Figure 6. Overall, an increase in size leads to a lowering of the E_{att}, with the sole outlier of $Mo_{32}C_{32}$, which has as a different signature displaying a di-σ-CM C_2H_4 mode, while others have a π-M mode. Indeed, the second most stable structure in $Mo_{32}C_{32}$ is a π-M mode, shown in gray color in Figure 6, and nicely fitting to the trend, to the point of being almost linear with a regression coefficient, R^2, of 0.96. Another distinct point for $Mo_{32}C_{32}$ is that the E_{dis} relates to a decrease of charge for the adsorbed C_2H_4 moiety, given the formation of a C–C covalent bond, see CDD and ELF plots in the Figure S2 of the SI.

Regarding Figure 5 again, one could argue that solely the $Mo_{24}C_{24}$ NP is an outlier in the observed trend. This exception may obey to its particular atomic structure. Even if while comparing to $Mo_{12}C_{12}$ both the adsorption mode and the *d*(CC) elongations are similar, the $Mo_{24}C_{24}$ NP is more symmetric, leading to a negligible NP distortion upon C_2H_4 adsorption, see Figure 6. However, the charge transfer from the MoC_y NP to the C_2H_4 molecule is quite large for $Mo_{12}C_{12}$ and $Mo_{24}C_{24}$ only; -0.30 *e* for both cases, while for Mo_6C_6 and $Mo_{32}C_{32}$ NPs the charge transfer from the adsorbate is below -0.15 *e*. Interestingly, the distortion energy is the same, 0.30 eV, for both $Mo_{12}C_{12}$ and $Mo_{24}C_{24}$ NPs. Overall, the maximum in E_{ads} relates to the minimum in E_{dis}. Therefore, the different $Mo_{24}C_{24}$ behavior obeys to its strong stability, favoring a higher charge transfer towards C_2H_4, and requiring a lower energy for elongating the C_2H_4 C═C bond. In fact, among all the 14 evaluated NPs, the distortion of $Mo_{24}C_{24}$ NP is almost negligible. Furthermore, the use of another descriptor other than the adsorption energy could help to understand the trends from Mo_6C_6 to $Mo_{24}C_{24}$. An increase in size leads to a drop in E_{att}, following a clear linear trend, although with $R^2 = 0.90$ only, within the studied range, having a clearer behavior compared to the adsorption energy.

3.4. Analysis of C_2H_4 interaction with non-stoichiometric MoC_y NPs

Several of the studied NPs are non-stoichiometric, with a Mo/C ratio in the range of 0.67–2.00. Even though the diversity in terms of geometries and Mo/C ratios, the systems with Mo/C<1, see top of Figure 7, top, exhibit E_{ads} within the -1.78 to -1.98 eV range, *i.e.* in a narrow range of 0.20 eV. For the cases with Mo/C>1, the binding energy variations are in the -1.76 to -2.88 eV range, *i.e.* in a broader range of 1.12 eV. Clearly, a large diversity is found for the latter cases. Aside from that, the decrease in the NPs size does not imply a clear trend in terms of the adsorption energy, and the only note of distinction are particular reconstructions as observed on the Mo_4C_6 and Mo_5C_6 NPs cases, see Figures S3 and S4 in the SI, forcing an sp^3 hybridization of C_2H_4 C atoms in the former, and the formation of C–C bonds in the latter. Notice that the catalyst reconstruction is an important issue that should be addressed, specially when in small NPs as recently reported by Sun *et al.*[51] Therefore, in further studies related to ethylene hydroconversion, the NPs reconstruction must be considered, particularly for the smallest ones.

For four Mo/C ratios —0.67, 0.83, 1.20, and 1.50—, there are particularly two different structures for each case, with different size; e.g. Mo_5C_6 and $Mo_{10}C_{12}$ for the case of Mo/C = 0.83. As generally seen in the top of Figure 3, the larger the size —in terms of C content—, the weaker the C_2H_4 binding energy, where by doubling the size the E_{ads} weakens ~0.2 eV, except for the Mo/C=1.50

ratio, where the drop is ~1 eV. Thus, it seems that size effects get pronounced particularly at Mo/C ratio larger than 1.20. Even though the major change in E_{ads} corresponds to NPs with Mo/C=1.50 ratio, E_{def} values are merely 0.06 eV; quite small compared to the values for Mo/C=0.83 of 0.58 eV, see top of Figure 3. This difference seems to be linked to a different adsorption mode. For Mo/C=1.50, the C_2H_4 binding mode is π-M, while for Mo/C=0.83 di-σ-CC and di-σ-CM modes. The C_2H_4 interaction on 75% of the non-stoichiometric NPs has a distortion energy of ~0.2 eV, in the range of ratio Mo/C = 0.67–2.00, with the sole exception of Mo_6C_4, that with a deformation energy of 0.07 eV could be negligible, implying an almost rigid NP structure upon C_2H_4 adsorption.

Among the evaluated NPs, E_{dis} is above 1 eV for several cases, which may not be advantageous for further hydrogenation reactions as could imply the breaking of the C═C bond. However, E_{dis} is lower than 0.53 eV for the particular Mo/C ratios of 0.67, 1.00, and 1.08. It is worth to mention that E_{dis} and E_{att} follow a similar trend as a function of Mo/C ratio. Hence, E_{att} depends on E_{dis}, which is thus a better descriptor than the adsorption energy. Therefore, the NPs attachment energies should also follow *Le Sabatier*'s principle, *i.e.* the C_2H_4 binding should be not too strong, as ethylene could remain molecularly adsorbed or dissociated on the NP, nor too weak, as C_2H_4 could not get hydrogenated. Moreover, C_2H_4 should bind on the MoC_y NPs with moderate activated E_{dis} while having a low NP deformation, E_{def}. The NPs which comply with the previous criteria are Mo_4C_6, Mo_8C_{12} (MetCar) and $Mo_{14}C_{13}$ (Nanocube), together with stoichiometric Mo_6C_6, $Mo_{12}C_{12}$, and $Mo_{24}C_{24}$ systems.

Aside from the previous considerations, the interaction of C_2H_4 with the NP triggers a charge transfer from the NP to ethylene, see bottom of Figure 7. Such accumulated charge in the adsorbed C_2H_4 increases with the Mo/C ratio, *i.e.* with an enrichment of Mo atoms in the system. Indeed, the amount of Mo in the NPs modulates their activity towards different elements in diverse chemical environments.[24] This behavior relates to the NP E_{def} and C_2H_4 E_{dis} energies, with an oscillating profile, pointing to a convergence towards the surface for bigger sizes, see Figure S5 of the SI. This rapidly oscillating behavior is typical of small NPs,[29] but increasing the number of Mo favors convergence, particularly from $Mo_{12}C_6$ onwards.

Focusing on the largest non-stoichiometric NPs, *i.e.* the $Mo_{12}C_x$, the Mo enrichment over the stoichiometric point modulates the chemical activity of Mo atoms towards the carbons of C_2H_4, as seen by a major extent of charge transfer from the NP Mo atoms towards C_2H_4, see bottom of Figure 7. For the $Mo_{12}C_x$ based NPs, the increase of the Mo/C ratio leads to a rise in the E_{ads}, see top of Figure S6 in the SI. In other words, the NP size decrease and the larger share of Mo atoms leads to an increase of the C_2H_4 adsorption. The C═C bond in C_2H_4 gets also activated in $Mo_{12}C_x$ systems, but its extent is different only for the stoichiometric NP, being 0.09 Å, and similar for the rest of ratios, in the 0.15–0.17 Å range. This behavior is also related to the E_{dis}, which in turn relates to the

Bader charge on the adsorbate, see Figure S6 in the SI, showing that an increase in the Mo/C ratio favors a higher charge transfer from the NPs to C_2H_4.

above 1.08 are not advantageous for activating C_2H_4, even if key in hydrogenation processes. Increasing the Mo/C ratio up to 1.5 implies higher E_{def} and E_{dis} with concomitant lower E_{att} as in going from $Mo_{12}C_6$ to $Mo_{12}C_{12}$. Therefore, the only desired ratios to bind ethylene are 1.00 and 1.08, *i.e.* having only a small content of C-deficiencies or, in other words, as close to stoichiometry as possible.

The results for the MetCar highlight another complex interplay between the Mo/C ratio and the chemical properties of a MoC_y NP. In this C-rich system, there are 1.5 atoms of C per each Mo atom, but the special structure and electronic properties of the NP allow it to bind ethylene better than δ-MoC(001) or β-Mo_2C(001)-C surfaces. In the structure of the MetCar, Figures 1 and 2, multiple bonds exist between the carbon atoms and the system exhibits C_2 dimers. It has been argued that the presence of C_2 dimers leads to special chemical properties.[52,53] With the exception of Mo_4C_6, C_2 dimers are not present in the other MoC_y NPs examined neither in the bulk δ-MoC(001) nor in β-Mo_2C(001) surfaces. Nevertheless, it is worth to mention that the C_2 dimers in Mo_4C_6 and the MetCar have different nature. In Mo_4C_6 these are formed upon interaction with ethylene as product of a significant structural rearrangement, see Figure S4 in SI, with a concomitant energy lowering of 0.6 eV. On the contrary, the isolated MetCar structure already contains C_2 dimers and, upon interaction with C_2H_4, the structure is not reconstructed. Therefore, the reactivity of the MetCar obeys not only to the presence of C_2 dimers, but also to its particular pyramidal-like geometry. Among the evaluated NPs, only Mo_4C_6 and Mo_5C_6 (the smallest ones) suffer changes in cluster geometry upon C_2H_4 adsorption which is a typical behavior in small size clusters. In fact, this behavior was not seen in the larger NPs Thus, in C-poor and C-rich MoC_y NPs, there are phenomena which are not possible in a bulk surface and can lead to high reactivity towards ethylene.

3.5. Electronic structure organization

The electron density rearrangement between the MoC_y NPs and the C_2H_4 molecule is further illustrated by the Bader atoms-in-molecules analysis in Figure 6 —and also Figure S6 of the SI—. This is here complemented by CDD and ELF analyses. Four representative NPs were taken, since they embody different adsorption modes and Mo/C ratios, leading to descriptors differences as above explained. The chosen NPs are $Mo_{12}C_6$ (σ-M, μ-M), $Mo_{12}C_{12}$ (π-M), $Mo_{10}C_{12}$ (di-σ-CM), and Mo_5C_6 (di-σ-CC), with Mo/C ratios of 2.00, 1.00, and 0.83 for two last cases, respectively.

The CDD and ELF plots for the adsorption on metal sites *via* π-M and σ-M, μ-M modes are displayed in Figure 8. The binding *via* σ-M, μ-M mode favors a high charge migration from the NP towards C_2H_4, as shown by the accumulation regions within the adsorbate, also observable in the *ELF* plot. Indeed, this high electron density correlates with the Bader charge of -0.61 *e*. Overall, the largest adsorbate charges were seen for the σ-M, μ-M binding mode. On the contrary, the adsorption *via* π-M mode has less electron density within the C_2H_4, in accordance with the smaller Bader charge of -0.30 *e*. Such a behavior may indicate that the C_2H_4 adsorption on the MoC_y NPs has some ionic contribution to the bonding.

The aforementioned electron density migration occupies the C_2H_4 Lowest Unoccupied Molecular Orbital (*LUMO*) antibonding orbitals, decreasing the bond order, and, consequently, elongating the C–C bond length. Indeed, the extent of the Bader charge relates to the *d*(CC) increase, as binding *via* σ-M, μ-M mode is higher, ranging 0.15 – 0.18 Å, compared to the binding *via* π-M mode, with increases of *ca.* 0.10 Å. The largest *d*(CC) elongation is seen on MoC_y- $C_{ethylene}$ sites, *i.e.* binding *via* di-σ-CX —X = C or Mo. This is a direct consequence of the formation of new C-C covalent bond with the NP C atom, as clearly seen in the CDD and ELF plots of Figure S7 in the SI, even if one has to regard that coulombic interactions play a role. Notice that on Mo_5C_6 not only *d*(CC) is elongated, but a sp^3 hybridization emerges due to a molecular distortion. This explains the highest E_{dis} of 3.68 eV, among the evaluated NPs, see Table S6 of the SI.

The ethylene binding on the NPs and on the extended δ-MoC(001) surface via π-M mode has clear differences in terms of charges, see Figure S8 of the SI. In the δ-MoC(001) surface there is a continuous flux of electron density within the layers[17] a general behavior seen on other TMCs.[45] The electronic arrangement between Mo and C atoms is perturbed upon C_2H_4 adsorption leading to an almost negligible *d*(CC) elongation of 0.03 Å, with both ionic and covalent contributions. On the NPs the electron density is more affected, due to the stronger adsorption, higher Bader charge in C_2H_4, and a larger *d*(CC) elongation of 0.09–0.25 Å.

4. Conclusions

The present systematic DFT study analyzed the ethylene binding on a series of MoC_y NPs, considering a broad Mo/C ratio range of 0.67–2.00. Overall, 14 NPs have been explored with structures derived from a cascade procedure. The most stable structures were then used to analyze C_2H_4 adsorption sampling *ca.* 500 adsorptive sites. The results show that a general classification can be established of the C_2H_4 binding related to the C–C bond length elongation and the NP active site. Thus, Group I is for π-M mode adsorption, Group II is for σ-M, μ-M mode and, finally, Group III involves NP C sites, *via* di-σ-CX —X = Mo, C. Overall, the C_2H_4 adsorption strongly affects the whole NP electron density, resulting in a stronger adsorption energy, higher negative charge on the

C_2H_4 adsorbate, and a d(CC) elongation of 0.09–0.25 Å, as compared to the respective behavior on an extended δ-MoC(001) surface, revealing a complex mixture of ionic and covalent bond.

The reported analysis involved differentiating stoichiometric and non-stoichiometric NPs, a decomposition of the interaction in terms of C_2H_4 distortion energy, NP deformation energy, and C_2H_4 attachment energy in a lock-&-key fashion, considering cohesive energies, Mo/C ratios, and the explicit number of MoC units as possible interaction descriptors. Thus, the NPs with low distortion, deformation, and attachment energies are the non-stoichiometric Mo_4C_6, Mo_8C_{12} (MetCar), and $Mo_{14}C_{13}$ (Nanocube), together with the stoichiometric Mo_6C_6, $Mo_{12}C_{12}$, and $Mo_{24}C_{24}$ NPs. These are promising systems to further support on metal surfaces, in a closer approach to a practical catalyst. The best predicted performance for C_2H_4 binding is for a Mo/C ratio below 1.08, as larger ratios are not advantageous for distorting C═C bond, which is key in the hydrogenation processes. The reasons rely on the above-mentioned descriptors analysis, accompanied by a geometric issue at high Mo/C ratios above 1.1, as an excess of Mo atoms leads to a lower coordination of Mo atoms, which is not advantageous since Mo binds C_2H_4 just to compensate its under-coordination, instead of favoring the C_2H_4 C–C lengthening, thus ultimately limiting its performance towards further hydrogenation reactions.

Conflicts of interest

The authors declare no conflict of interest.

Acknowledgments

The research carried out at the Universitat de Barcelona has been supported by the Spanish MICIUN RTI2018-095460-B-I00 and *María de Maeztu* MDM-2017-0767 grants, and, in part, by *Generalitat de Catalunya* 2017SGR13 grant and COST Action CA18234. C. J.-O. and E. F. acknowledge to *Universidad de Medellín* for financial support under the internal project 1143. F. I. acknowledges additional support from the 2015 ICREA Academia Award for Excellence in University Research. Part of this research used resources of the Center for Functional Nanomaterials, which is a U.S. DOE Office of Science Facility, and the Scientific Data and Computing Center, a component of the Computational Science Initiative, at Brookhaven National Laboratory under Contract No. DE-SC0012704.

Supporting Information for Publication

The Supporting Information is available free of charge at DOI:

Table S1. Total energy difference between the lowest and second lowest structures per stoichiometry.

Table S2. Formation energies, E_{form}, for each stoichiometric NP per MoC unit and band gap related energies.

Table S3. Band gap energy, E_{gap}, for the non-stoichiometric MoC_y NPs.

Table S4. Adsorption of C_2H_4 on MoCy NPS.

Table S5. Two most stable C_2H_4 adsorption energies and structures on every MoC_y NP.

Table S6. Energy contributions to the C_2H_4 adsorption energy on the different studied MoC_y NPs.

Table S7. Cohesive energies for the studied stoichiometric MoC NPs.

Figure S1. Formation energies per MoC unit for each of the studied stoichiometric MoC NPs as a function of the MoC units.

Figure S2. CDD and ELF for the C_2H_4 binding on $Mo_{32}C_{32}$ NP.

Figure S3. Geometry changes in the Mo_5C_6 NP upon C_2H_4 adsorption.

Figure S4 Geometry changes in the Mo_4C_6 NP upon C_2H_4 adsorption.

Figure S5. NP deformation energy and C_2H_4 distortion energy on non-stoichiometric NPs sorted relative to the amount of Mo in the explored NPs.

Figure S6. Effect of Mo/C ratio of $Mo_{12}C_x$ NPs in adsorption energy and size.

Figure S7. CDD and ELF for the C_2H_4 binding through di-σ-CC on Mo_5C_6 NP

Geometry coordinates of bare NPs and C_2H_4 adsorbed on them

Table 1. Adsorption energy, E_{ads}, for the ethylene adsorption on the studied MoC_y nanoparticles, for the most-stable site, and evaluating the distortion (activation) by the C_2H_4 C=C bond length, *d*(CC). Energy values include the ZPE contribution. Reference data on most stable δ-MoC(001) and β-Mo_2C(001) surfaces, either C- or Mo-terminated, as provided.

MoC_y	**Site**	**E_{ads} / eV**	***d*(CC) / Å**
Stoichiometric			
Mo_6C_6	π-M	-1.76	1.43
$Mo_{12}C_{12}$	π-M	-1.65	1.42
$Mo_{24}C_{24}$	π-M	-1.84	1.42
$Mo_{32}C_{32}$	di-σ-CM	-1.54	1.55
Non-stoichiometric			
Mo_4C_6	π-M	-1.98	1.44
Mo_5C_6	di-σ-CC	-1.97	1.56
Mo_6C_4	σ-M, μ-M	-2.88	1.51
Mo_6C_5	σ-M, μ-M	-1.99	1.51
Mo_8C_{12}	π-M	-1.80	1.43
$Mo_{10}C_{12}$	di-σ-CM	-1.78	1.58
$Mo_{12}C_6$	σ-M, μ-M	-2.08	1.48
$Mo_{12}C_8$	σ-M, μ-M	-1.86	1.49
$Mo_{12}C_{10}$	σ-M, μ-M	-1.76	1.50
$Mo_{14}C_{13}$	π-M	-1.85	1.44
Surfaces References			
δ-MoC(001)[a]	π-M	-0.44[c]	1.36
β-Mo_2C(001)-C[b]	C-top, Mo-h_1	-1.49	1.51
β-Mo_2C(001)-Mo[b]	Mo-top, C-h_2	-2.50	1.48

[a] Refs.[17,19] , [b] Ref.[18], [c] reoptimized using present computational set-up. See complete table in Table S4, SI.

Figure 1. Geometry for the bare MoC_y NPs The Mo and C atoms are represented by magenta and brown color, respectively.

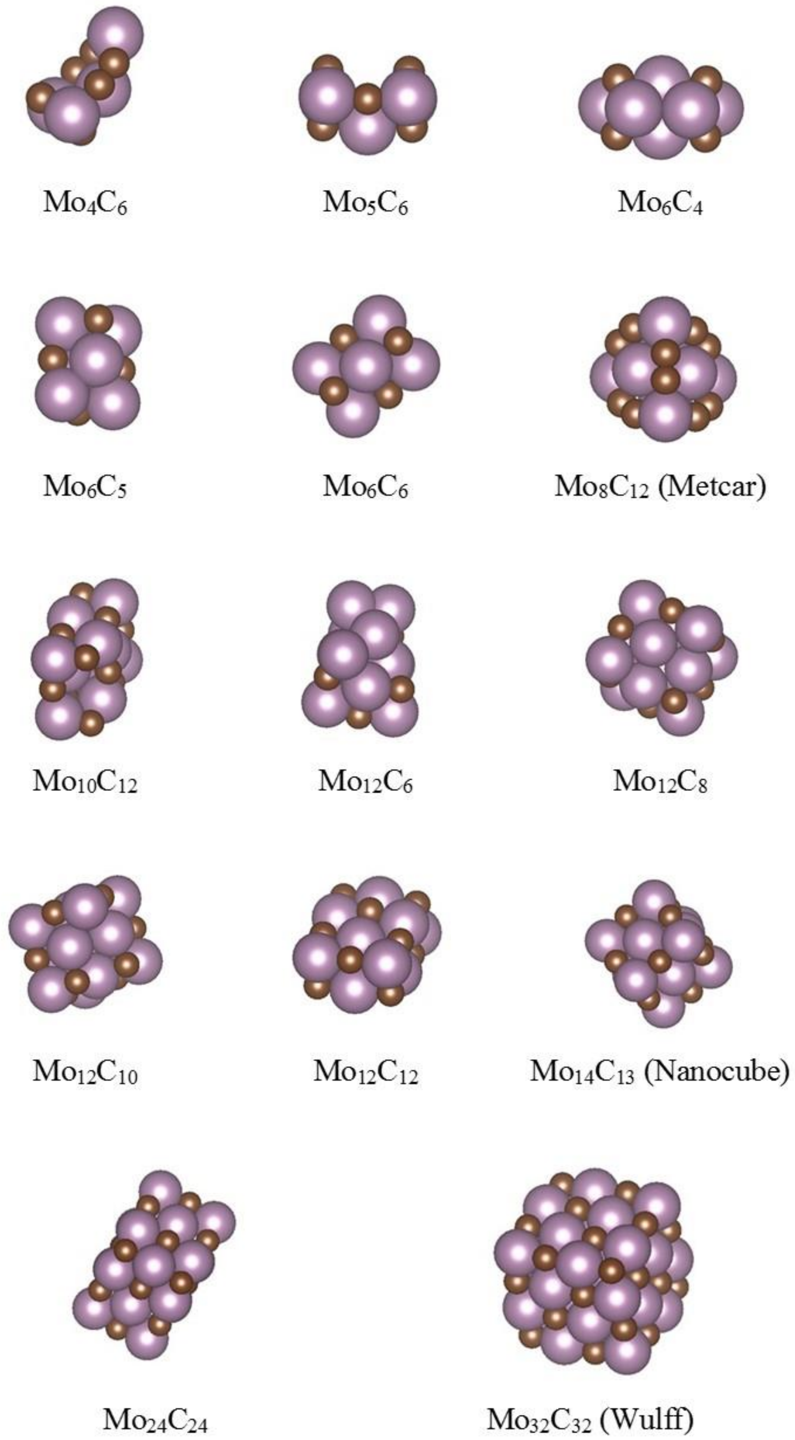

Figure 2. Most stable geometry of C_2H_4 adsorbed on every NP. The Mo, C, and H atoms are represented by magenta, brown, and light gray, respectively. The binding mode is tagged along the structure.

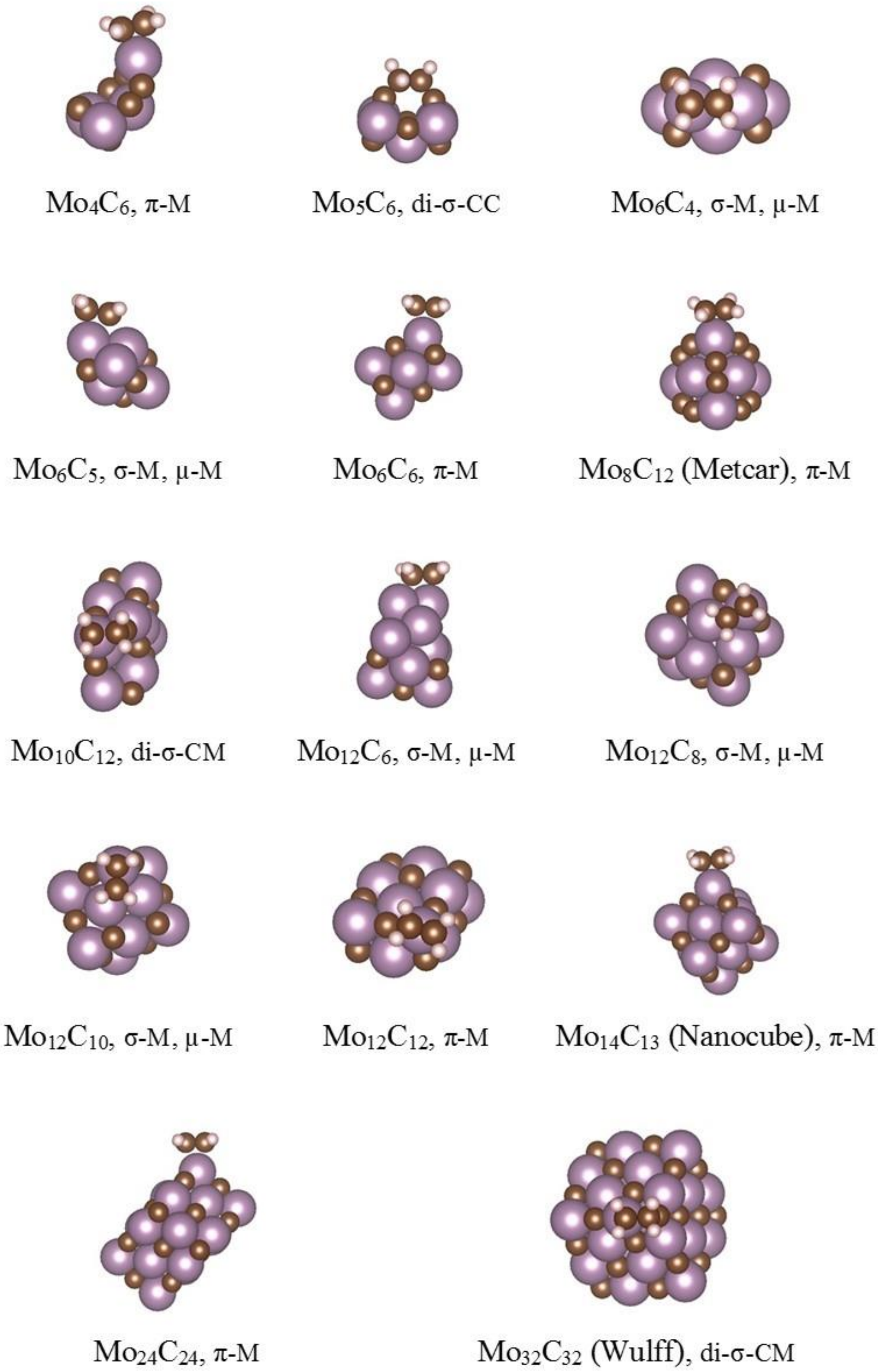

Figure 3 Adsorption energies, E_{ads}, for the most stable C_2H_4 structure adsorbed in every NP, sorted in terms of the energy strength. Extended surface values are shown as references.

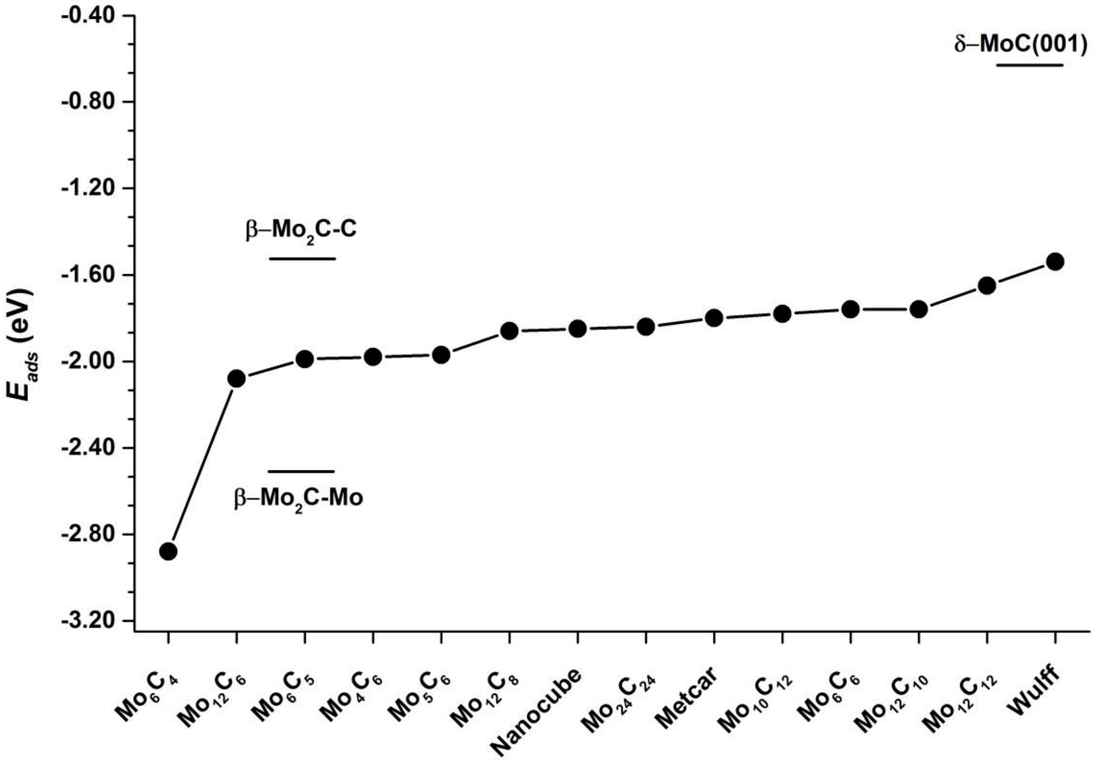

Figure 4 Comparative geometry binding of C_2H_4 on NPs and surfaces for the four adsorption modes found on NPs.

Adsorption mode	MoC_y NP	δ-MoC(001)	β-Mo_2C(001)-C	β-Mo_2C(001)-Mo
π-M		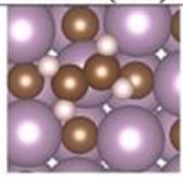	N.A.	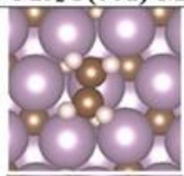
σ-M, μ-M		N.A.	N.A.	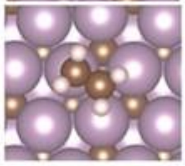
di-σ-CM		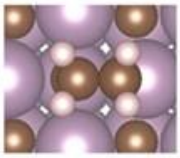	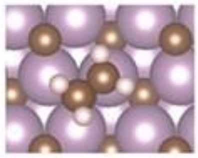	N.A.
di-σ-CC		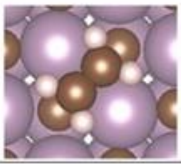	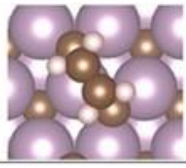	N.A.

Figure 5. C_2H_4 adsorption on stoichiometric NPs (red points), while values on related non-stoichiometric NPs (black points) are shown in insets.

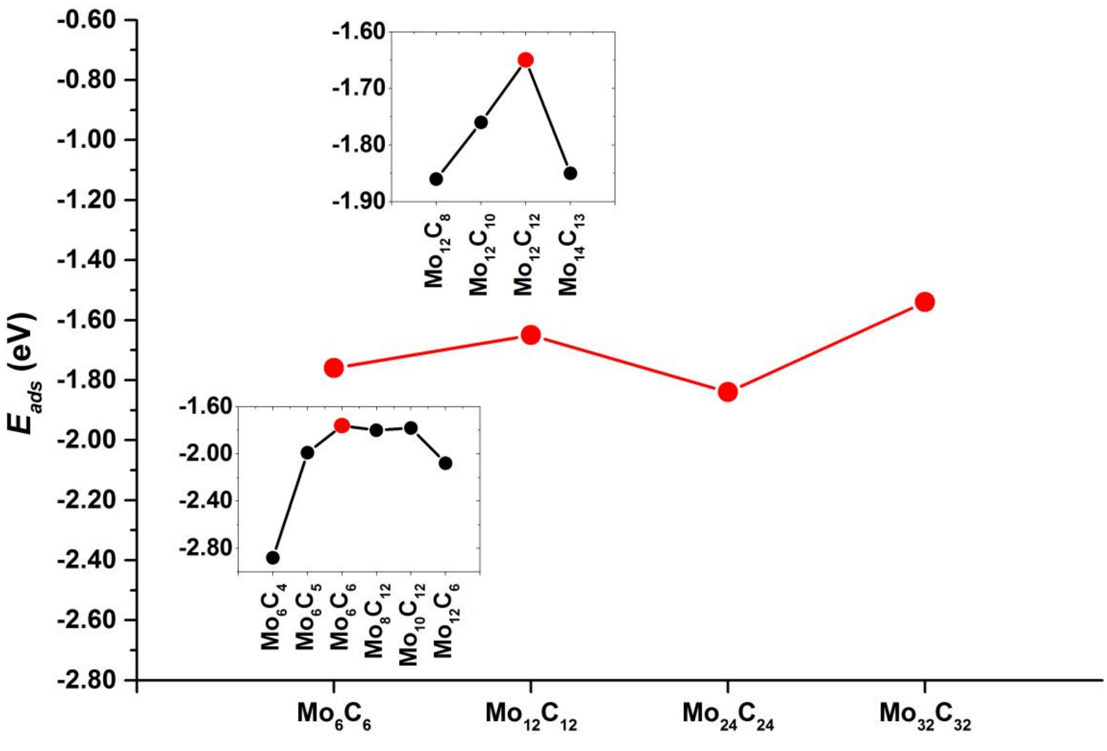

Figure 6. Left panel: Evolution with respect size, measured as $N^{-1/3}$, of the attachment energy, E_{att}. The second most stable structure for $Mo_{32}C_{32}$ is shown in gray. Right panel: Bader charge, Q, C_2H_4 distortion energy, E_{dis}, and NP deformation energy, E_{def}.

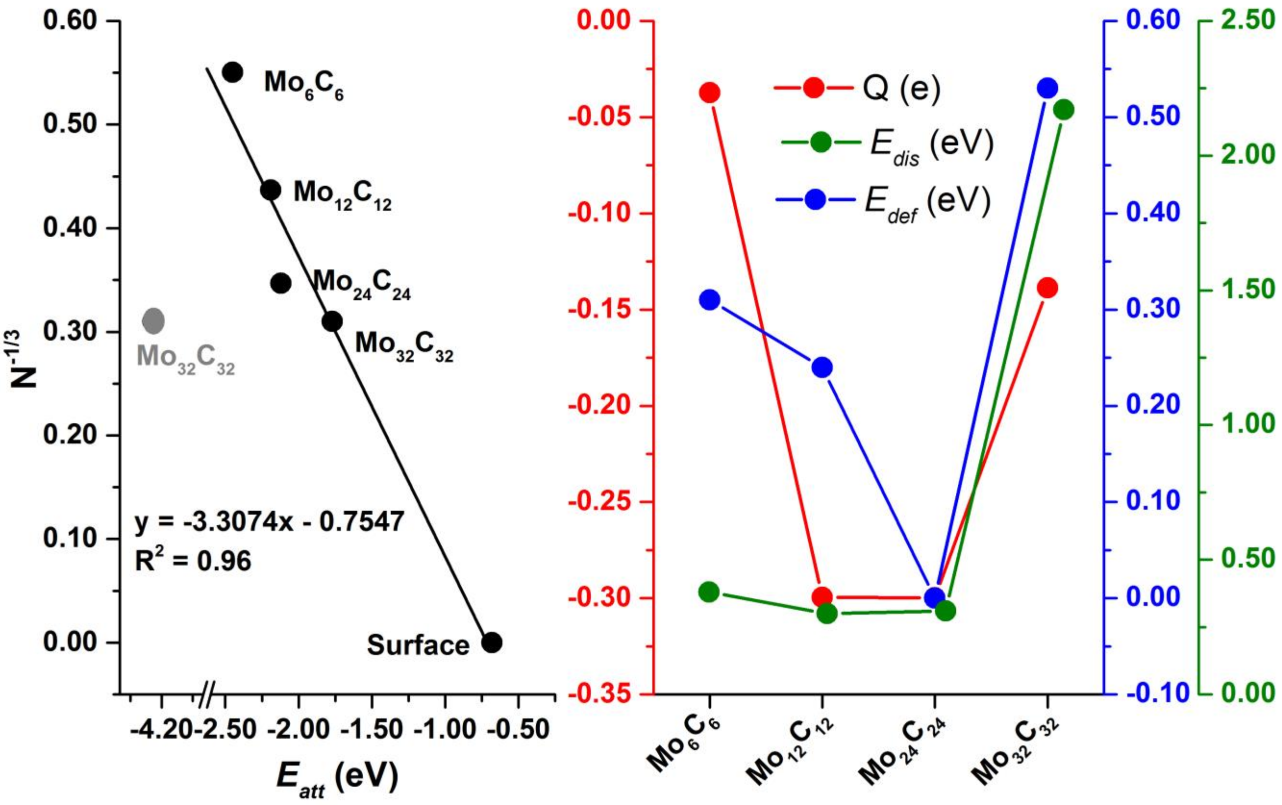

Figure 7. Effect of Mo/C ratio in non-stoichiometric NPs on the adsorption energy, E_{ads}, and NP deformation energy, E_{def} (upper panel). Adsorbed C_2H_4 Bader charge (in e), C_2H_4 distortion energy E_{dis}, and ethylene attachment energy, E_{att} (lower panel), both in eV.

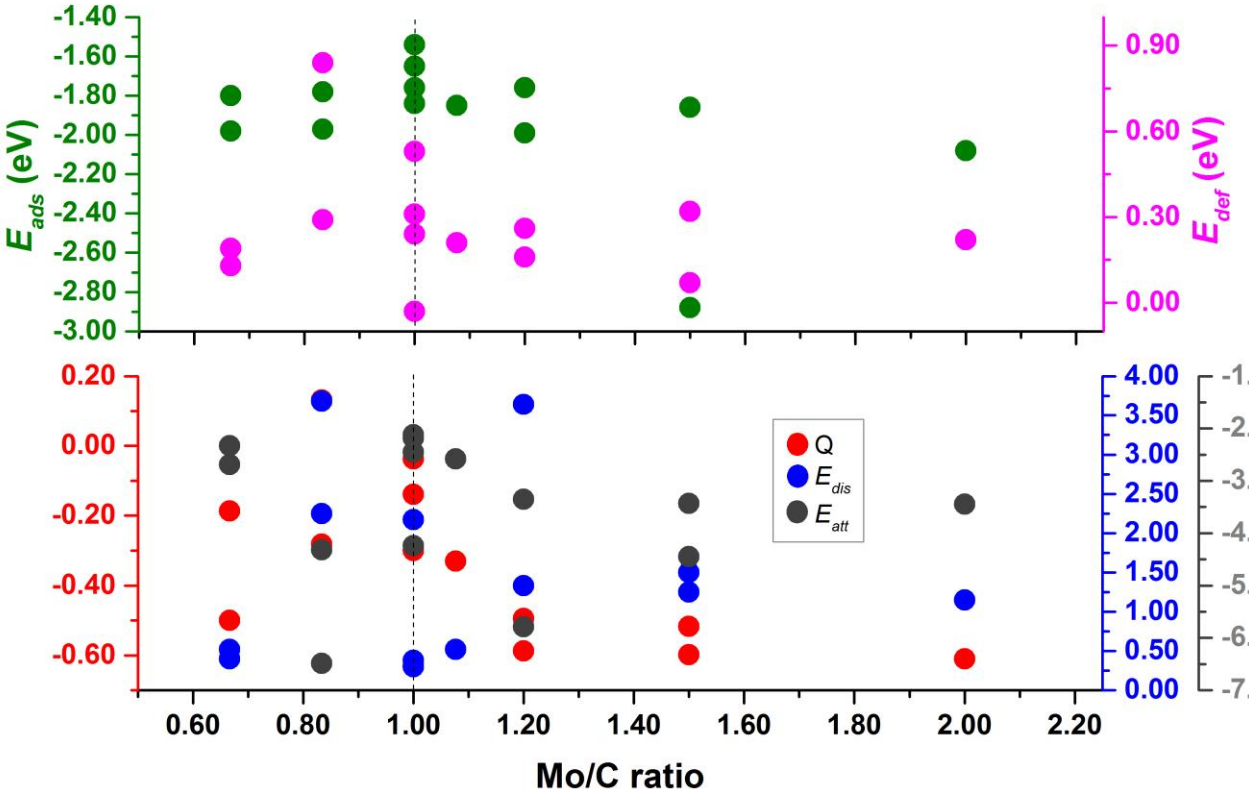

Figure. 8. CDD plot (top) and ELF (bottom) for binding *via* a) σ-M, μ-M ($Mo_{12}C_6$), E_{ads} = -2.08 eV; b) π-M mode ($Mo_{12}C_{12}$), E_{ads} = -1.65 eV. For the CDD, red and green colors represent the regions where the charge (0.05 e/Å^3) was lost and earned, respectively, after ethylene adsorption. The Mo, C, and H atoms are represented by magenta, brown and light gray color, respectively. In the ELF, blue, green, and red colors represent low (0), intermediate (0.5), and high (1) likelihood of finding electron pair, respectively.

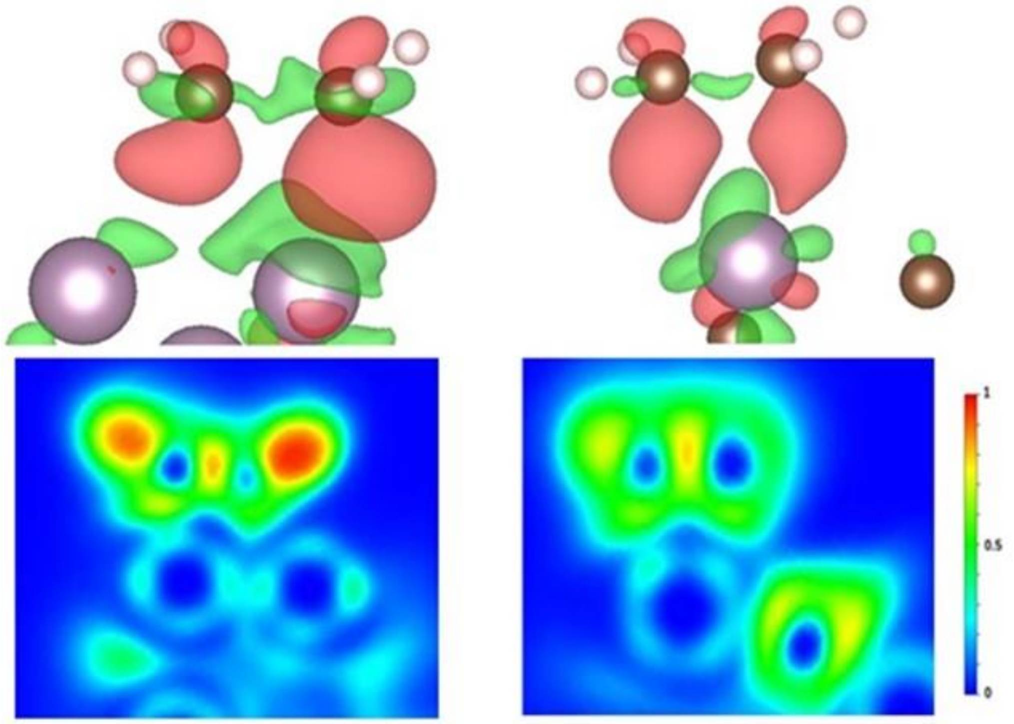

a) b)

References

(1) Wilson, J. N.; Otvos, J. W.; Stevenson, D. P.; Wagner, C. D. Hydrogenation of Olefins over Metals. *Ind. Eng. Chem.* **1953**, *45*, 1480–1487.

(2) Dhandapani, B.; St. Clair, T; Oyama, S. T. Simultaneous Hydrodesulfurization, Hydrodeoxygenation, and Hydrogenation with Molybdenum carbide *Appl. Catal. A: Gen.* **1998**, *168*, 219–228.

(3) Bus, E.; Ramaker, D. E.; van Bokhoven, J. A. Structure of Ethene Adsorption Sites on Supported Metal Catalysts from in Situ XANES Analysis. *J. Am. Chem. Soc.* **2007**, *129*, 8094–8102.

(4) Binder, A.; Seipenbusch, M.; Muhler, M.; Kasper, G. Kinetics and Particle Size Effects in Ethene Hydrogenation Over Supported Palladium Catalysts at Atmospheric Pressure. *J. Catal.,* **2009**, *268*, 150–155.

(5) Tsung, C.; Kuhn, J. N.; Huang, W.; Aliaga, C.; Hung, L.; Somorjai, G. A.; Yang, P. Sub-10 nm Platinum Nanocrystals with Size and Shape Control: Catalytic Study for Ethylene and Pyrrole Hydrogenation. *J. Am. Chem. Soc.* **2009**, *131*, 5816–5822.

(6) Aboul-Gheit, A. K.; Aboul-Fotouh, S. M.; Aboul-Gheit, N. A. K. Hydroconversion of Cyclohexene Using Catalysts Containing Pt, Pd, Ir, and Re Supported on H-ZSM-5 Zeolite. *Appl. Catal. A: Gen.* **2005**, *283*, 157–164.

(7) Sapi, A.; Thompson, C.; Wang, H.; Michalak, W. D.; Ralston, W. T.; Alayoglu, S.; Somorjai, G. A. Recovery of Pt Surfaces for Ethylene Hydrogenation-Based Active Site Determination. *Catal. Lett.* **2014**, *144*, 1151–1158.

(8) Rioux, R. M.; Komor, R.; Song, H.; Hoefelmeyer, J. D.; Grass, M.; Niesz, K.; Yang, P.; Somorjai, G. A. Kinetics and Mechanism of Ethylene Hydrogenation Poisoned by CO on Silica-supported Monodisperse Pt Nanoparticles. *J. Catal.* **2008**, *254*, 1–11.

(9) Cunha, D. S.; Cruz, G. M. Hydrogenation of Benzene and Toluene Over Ir Particles Supported on γ-Al_2O_3. *Appl. Catal. A: Gen.* **2002**, *236*, 55–66.

(10) Guil, J. M.; Masiá, A. P.; Paniego, A. R.; Menayo, J. M. T. Energetics of H_2 and O_2 Adsorption on Ir/γ-Al_2O_3 and Ir/SiO_2 Catalysts. Dependence on Support and on Metal Particle Size. *Thermochimica Acta* **1998**, *312*, 115–124.

(11) Piegsa, A.; Korth, W.; Demir, F.; Jess, A. Hydrogenation and Ring Opening of Aromatic and Naphthenic Hydrocarbons Over Noble Metal (Ir, Pt, Rh)/Al_2O_3 Catalysts. *Catal. Lett.* **2012**, *142*, 531–540.

(12) Levy, R. B.; Boudart, M. Platinum-Like Behavior of Tungsten Carbide in Surface Catalysis. *Science* **1973**, *181*, 547–549.

(13) Ardakani, S. J.; Liu, X.; Smith, K. J. Hydrogenation and Ring Opening of Naphthalene on Bulk and Supported Mo_2C Catalysts. *Appl. Catal. A: Gen.* **2007**, *324*, 9–19.
(14) Hwu, H. H.; Chen, J. G. Surface Chemistry of Transition Metal Carbides. *Chem. Rev.* **2005**, *105*, 185–212.
(15) Posada-Pérez, S.; Viñes, F.; Ramirez, P. J.; Vidal, A. B.; Rodriguez, J. A.; Illas, F. The Bending Machine: CO_2 Activation and Hydrogenation on δ-MoC(001) and β-Mo_2C(001) Surfaces. *Phys. Chem. Chem. Phys.* **2014**, *16*, 14912–14921.
(16) Rocha, A. S.; Rocha, A. B.; Teixeira, V. Benzene Adsorption on Mo_2C: A Theoretical and Experimental Study. *Appl. Catal. A: Gen.* **2010**, *379*, 54–60.
(17) Jimenez-Orozco, C.; Florez, E.; Moreno, A.; Liu, P; Rodriguez, J. A. Systematic Theoretical Study of Ethylene Adsorption on δ-MoC(001), TiC(001), and ZrC(001) Surfaces. *J. Phys. Chem. C* **2016**, *120*, 13531–13540.
(18) Jimenez-Orozco, C.; Florez, E.; Moreno, A.; Liu, P.; Rodriguez, J. A. Acetylene and Ethylene Adsorption on a β-Mo_2C(100) Surface: A Periodic DFT Study on the Role of C- and Mo-Terminations for Bonding and Hydrogenation Reactions. *J. Phys. Chem. C* **2017**, *121*, 19786–19795.
(19) Jimenez-Orozco, C.; Flórez, E.; Viñes, F.; Rodriguez, J. A; Illas, F. Critical Hydrogen Coverage Effect on the Hydrogenation of Ethylene Catalyzed by δ-MoC(001): An *Ab Initio* Thermodynamic and Kinetic Study. *ACS Catal.* **2020**, *10*, 6213–6222.
(20) Jimenez-Orozco, C.; Flórez, E.; Moreno, A.; Rodriguez, J. A. Platinum *vs.* Transition Metal Carbide Surfaces as Catalysts for Olefin and Alkyne Conversion: Binding and Hydrogenation of Ethylidyne. *J. Phys.: Conf. Ser.* **2019**, *1247*, 012003.
(21) Figueras, M.; Jurado, A.; Morales-Garcia, Á.; Viñes, F.; Illas, F. Bulk (in)stability as a Possible Source of Surface Reconstruction. *Phys. Chem. Chem. Phys.* **2020**, *22*, 19249–19253.
(22) Figueras, M.; Gutiérrez, R. A.; Viñes, F.; Ramírez, P. J.; Rodriguez, J. A.; Illas, F. Supported Molybdenum Carbide Nanoparticles as Hot Hydrogen Reservoirs for Catalytic Applications. *J. Phys. Chem. Lett.* **2020**, *11*, 8437–8441.
(23) Horn, J. M.; Song, Z.; Potapenko, D. V.; Hrbek, J.; White, M. G. Characterization of Molybdenum Carbide Nanoparticles Formed on Au(111) Using Reactive-Layer Assisted Deposition. *J. Phys. Chem. B* **2005**, *109*, 44.
(24) Gao, J.; Zheng, Y.; Fitzgerald, G. B.; de Joannis, J.; Tang, Y.; Wachs, I. E.; Podkolzin, S. G. Structure of Mo_2C_x and Mo_4C_x Molybdenum Carbide Nanoparticles and Their Anchoring Sites on ZSM-5 Zeolites. *J. Phys. Chem. C*, **2014**, *118*, 4670–4679.
(25) N. Vo, Dai-Viet; Adesina, A. A. Fischer–Tropsch synthesis over alumina-supported molybdenum carbide catalyst. *Applied Catalysis A: General*, **2011**, *399*, 221–232.

(26) Shou, Heng; Davis, R. J. Multi-product steady-state isotopic transient kinetic analysis of CO hydrogenation over supported molybdenum carbide. *Journal of Catalysis*, **2013**, *306*, 91–99.

(27) Baddour, F. G.; Roberts, E. J.; To, A. T.; Wang, L.; Habas, S. E.; Ruddy, D. A.; Bedford, N. M.; Wright, Joshua; Nash, C. P.; Schaidle, J. A.; Brutchey, R. L.; Malmstadt, N. An Exceptionally Mild and Scalable Solution-Phase Synthesis of Molybdenum Carbide Nanoparticles for Thermocatalytic CO_2 Hydrogenation. *J. Am. Chem. Soc.,* **2020**, 142, 1010–1019.

(28) Lamiel, O.; Bromley, S. T.; Illas, F. Low-energy Nanoscale Clusters of $(TiC)_n$ n = 6, 12: A Structural and Energetic Comparison with MgO. *Theor. Chem. Acc*. **2013**, *132*, 1312.

(29) Viñes, F.; Gomes, J. R. B.; Illas, F. Understanding the Reactivity of Metallic Nanoparticles: Beyond the Extended Surface Model for Catalysis. *Chem. Soc. Rev.* **2014**, *43*, 4922–4939.

(30) Quesne, M.; Roldán, A.; De Leeuw, N. H.; Catlow, C. R. A. Bulk and surface properties of metal carbides: implications for catalysis. *Chem. Soc. Rev.* **2018**, *20*, 6905–6916.

(31) Viñes, F.; Sousa, C.; Liu, P.; Rodriguez, J. A.; Illas, F. A systematic Density Functional Theory Study of the Electronic Structure of Bulk and (001) Surface of Transition-metals Carbides *J. Chem. Phys.* **2005**, *122*, 174709.

(32) Guo, B. C.; Kerns, K. P.; Castleman Jr., A. W. Ti_8C^{12+}-Metallo-Carbohedrenes: A New Class of Molecular Clusters? *Science* **1992**, *255*, 1411.

(33) Pilgrim, J. S.; Ducan, M. A. Beyond Metallo-carbohedrenes: Growth and Decomposition of Metal-carbon Nanocrystals. *J. Am. Chem. Soc.* **1993**, *115*, 9724–9727.

(34) Kresse, G.; Furthmüller, J. Efficient Iterative Schemes for *ab initio* Total-energy Calculations Using a Plane-wave Basis Set. *Phys. Rev. B* **1996**, *54*, 11169–11186.

(35) Perdew, J. P.; Burke, K.; Ernzerhof, M. Generalized Gradient Approximation Made Simple. *Phys. Rev. Lett.* **1996**, *77*, 3865–3868.

(36) Politi, J. R. D. S.; Viñes, F.; Rodriguez, J. A.; Illas, F. Atomic and Electronic Structure of Molybdenum Carbide Phases: Bulk and Low Miller-index Surfaces. *Phys. Chem. Chem. Phys.* **2013**, *15*, 12617–12625.

(37) Grimme, S.; Antony, J.; Ehrlich, S.; Krieg, H. A consistent and accurate *ab initio* parametrization of density functional dispersion correction (DFT-D) for the 94 elements H-Pu. *J. Chem. Phys.* **2010**, *132*, 154104.

(38) Kunkel, C.; Viñes, F.; Illas, F. Transition Metal Carbides as Novel Materials for CO_2 Capture, Storage, and Activation. *Energy Environ. Sci.* **2016**, *9*, 141–144.

(39) Liu, X.; Kunkel, C.; Ramírez de la Piscina, P.; Homs, N.; Viñes, F.; Illas, F. Effective and Highly Selective CO Generation from CO_2 Using a Polycrystalline α-Mo_2C Catalyst. *ACS Catal*. **2017**, *7*, 4323–4335.

(40) Blöchl, P. E. Projector Augmented-wave Method. *Phys. Rev. B* **1994**, *50*, 17953–17979.
(41) Kresse, G.; Joubert, D. From ultrasoft pseudopotentials to the projector augmented-wave method. *Phys. Rev. B* **1999**, *59*, 1758–1775
(42) Ha, M.; Baxter, E. T.; Cass, A.; Anderson, S. L.; Alexandrova, A. N. Boron Switch for Selectivity of Catalytic Dehydrogenation on Size-Selected Pt Clusters on Al_2O_3. *J. Am. Chem. Soc*. **2017**, *139*, 11568–11575.
(43) Gorey, T. J.; Zandkarimi, B.; Li, G.; Baxter, E. T.; Alexandrova, A. N.; Anderson, S. L. Coking-Resistant Sub-Nano Dehydrogenation Catalysts: Pt_nSn_x/SiO_2 (n = 4, 7). *ACS Catal.* **2020**, 10, 4543–4558.
(44) Li, G.; Zandkarimi, B.; Cass, A.; Gorey, T. J.; Allen, B. J.; Alexandrova, A. N.; Anderson, S. L. Sn-modification of Pt_7/alumina model catalysts: Suppression of carbon deposition and enhanced thermal stability. *J. Chem. Phys.* **2020**, 152, 024702.
(45) Jimenez-Orozco, C.; Flórez, E.; Montoya, A.; Rodriguez, J. A. Binding and Activation of Ethylene on Tungsten Carbide and Platinum Surfaces. *Phys. Chem. Chem. Phys.* **2019**, *21*, 17332–17342.
(46) Bader, R. Atoms in Molecules: A Quantum Theory; Oxford University Press: New York, **1990**
(47) Bromley, S.; Moreira, I. P. R.; Neyman, K. M.; Illas, F. Approaching Nanoscale Oxides: Models and Theoretical Methods. *Chem. Soc. Rev.* **2009**, *38*, 2657–2670.
(48) Shen, J.; Hill, J. M.; Watwe, R. M.; Spiewak, B. E.; Dumesic, J. A. Microcalorimetric, Infrared Spectroscopic, and DFT Studies of Ethylene Adsorption on Pt/SiO_2 and $Pt\text{-}Sn/SiO_2$ Catalysts. J. *Phys. Chem. B*. **1999**, *103*, 3923–3934.
(49) Watwe, R. M.; Spiewak, B. E.; Cortright, R. D.; Dumesic, J. A. Density Functional Theory (DFT) Studies of C_1 and C_2 Hydrocarbons Species on Pt Clusters. *J. Catal*. **1998,** *180*, 184–193.
(50) Crampton, A. S.; Rötzer, M. D; Schweinberger, F. F.; Yoon B.; Landman, U.; Heiz, U.; Controlling Ethylene Hydrogenation Reactivity on Pt_{13} Clusters by Varying the Stoichiometry of the Amorphous Silica Support. *Angew. Chem. Int. Ed*. **2016**, 55, 8953–8957.
(51) Sun, G.; Fuller III, J. T.; Alexandrova, A. N.; Sautet, P. Global Activity Search Uncovers Reaction Induced Concomitant Catalyst Restructuring for Alkane Dissociation on Model Pt Catalysts. *ACS Catal.* **2021**, *11*, 1877–1885.
(52) Liu, P.; Rodriguez, J. A.; Muckerman, J. T. The Ti_8C_{12} Metcar: A New Model Catalyst for Hydrodesulfurization. *J. Phys. Chem. B*, **2004**, *108*, 18796 – 18798.
(53) Liu, P.; Rodriguez, J. A. Effects of carbon on the stability and chemical performance of transition metal carbides: A density functional study. *J. Chem. Phys.*, **2004**, *120*, 5414.

Graphic for TOC